ELECTRONIC TRANSPORT PROPERTIES OF $Fe(qsal)_2(TCNQ)_2$ MOLECULAR FILMS

by

Bryce Herrington

AN UNDERGRADUATE THESIS

Presented to the Faculty of

The College of Arts and Sciences

At the University of Nebraska

For the Degree of Bachelor of Science

Major: Physics

Under the Supervision of
Prof. Dr. Robert Streubel and Prof. Dr. Peter Dowben

Lincoln, Nebraska

March 2024

UNIVERSITY *of* NEBRASKA
LINCOLN

Contents

1 Abstract

It has been noted that the use of molecular magnet-based transistors within memory devices could potentially dramatically decrease the energy consumption of devices through both the lesser energy cost for molecular transistors and fewer total transistors needed per memory device. Previous work on Fe(qsal)$_2$(TCNQ)$_2$ molecules demonstrated sufficiently low energy cost and large spin-orbit coupling to be a promising candidate for application in devices. The aim of this work is to characterize the electrical impedance behavior of Fe(qsal)$_2$(TCNQ)$_2$ molecular films in the GHz frequency range necessary for the proposed devices connected to the read/write speed. Extrapolation of impedance trends in the MHz range corresponds to favorably low impedance in the desired frequency range. In addition, an RC circuit model was developed to explain the effective resistance and capacitive reactance behavior observed in impedance measurements and DC current-voltage characteristics. The indication of sufficient read/write speed motivates further characterization of the Fe(qsal)$_2$(TCNQ)$_2$ molecule.

2 Introduction

2.1 Motivation

Conventional memory devices that operate in the GHz range are rapidly increasing in demand, and the energy efficiency of such microelectronic devices must be drastically improved to avoid a crisis in energy consumption [1]. Though there have been steady improvements to the transistor technology within memory devices in the past, it is increasingly difficult to improve the size and energy efficiency using traditional mechanisms. Size and efficiency improvements to conventional transistor mechanisms encounter physical, technological, and financial limits. The $Fe(qsal)_2(TCNQ)_2$ molecule has spin-crossover characteristics, and the focus of this research was regarding the molecule as a molecular magnet within devices which could potentially supplant conventional devices and bypass the associated looming energy crisis entirely [5].

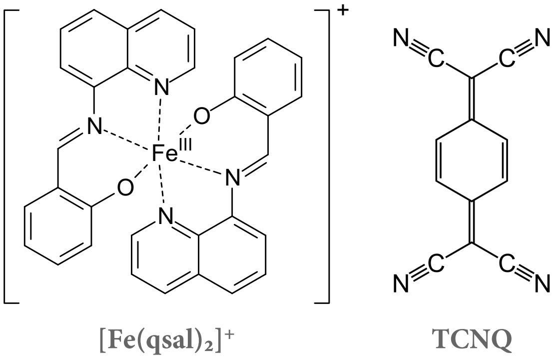

Fig. 2.1.1: *Diagram of* $Fe(qsal)_2$ *and TCNQ molecules.*

The size of conventional transistor gates cannot physically be decreased much farther beyond 5 nm, which indicates the end of Moore's law [4], the industry projection that the number of transistors per integrated circuit will increase exponentially with time. Over recent decades, the electronics industry has spent increasingly larger sums of money to match this "law", but not even these billions can override the inherent limt of the atomic scale [2]. Similarly, we can no longer increase the power density due to the more pronounced effects of heating at increasingly smaller scales [2]. Thus, if new technology is not development, our perpetually increasing utilization of transistor-based devices will spell disaster from the energy use perspective. If consumption trends continue to 2030, they will become unsustainable. Rather than continuing to solely focus on marginal improvements to existing technology, a novel physical mechanism could be exploited to circumvent the inherent limitations of conventional transistors. Molecular microelectronics represents such a potential replacement.

Molecular miccroelectronics utilizes the spin and magnetic moment of single molecules (often organic molecules [7]) to store information. With this mechanism, they can theoretically be used to create nonvolatile memory devices which do not require a sustained current/voltage in the idle state [3][5] and can reduce the necessary number of transistors per memory cell from 6 conventional transistors down to 2 transistors: 1 molecular and 1 conventional transistor acting as a switch for read/write operation. To take full advantage of the molecular magnet-based transistor in practice, a molecule must be found that behaves sufficiently well for several important parameters.

2.2 Scope of Thesis

With the goal of finding a well-behaving molecule for microelectronics applications in the GHz range, the $\mathrm{Fe(qsal)_2(TCNQ)_2}$ molecule have been shown to be a particularly promising candidate, with an extremely low energy cost < 5 aJ per read/write operation. Prior work of collaborators demonstrated unprecedented critical current density of 10^5 $\mathrm{A/cm^2}$ and a spin-orbit coupling of 0.5 eV yielding an on/off ratio of 6^5 well beyond the industry benchmark. Additionally, samples showed a resistance less than 1 Ωcm and a spin-orbit coupling exceeding 1.4 eV.

The switching behavior is derived from the high-frequency impedance. Thus, determining the impedance behavior of the molecule to characterize the read/write speed is the next crucial step in determining the likelihood of possible application. Without sufficient speed (low impedance in the desired range), molecular magnet-based technology would not be able to supplant conventional transistors within memory devices. We cannot directly measure in the GHz range (our limit for direct measurement is in the MHz range). Because the speed is size-dependent and may easily exceed the MHz range, trends fitted to data in the MHz range can be extended to the GHz range, i.e., points on the larger length scales (smaller time scales) were extrapolated to that of the known physical limits. This approach circumvents the probing limitations of experimentally accessible time and length scales at the University of Nebraska-Lincoln.

3 Experimental Methods

3.1 Synthesis and Fabrication

Samples were deposited via drop-casting using a solution of the molecules in methanol with a semi-conducting polymer synthesized by our chemistry collaborators. The sample solution using the methodology in [6], and the solution was then deposited onto Metrohm interdigiated gold electrode chips (see Fig. 3.1.1). The initial quality of drop-casted samples may have contributed to the tendency for sample degradation under repeated applications of direct currents around 20 nA.

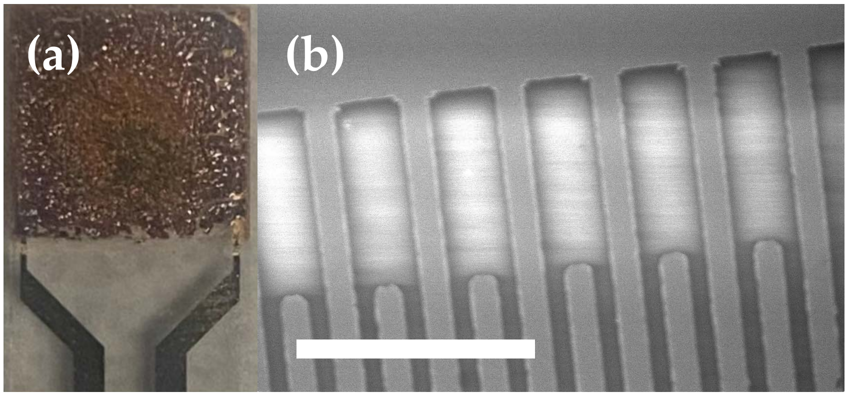

Fig. 3.1.1: *(a) Optical imge of the sample and (b) SEM image of bare Metrohm chip using in-lens detector. Length scale is 50 μm.*

When depositing, too thin of a layer resulted in cracked surfaces, and thick layers had uneven surfaces as seen with scanning electron microscopy (SEM) (Fig. 3.2.1). Therefore, creating the higher quality samples was an inconsistent process that could likely be improved by using spin-coating. The Metrohm chips consist of adjacent gold lines originating from oppositte electrodes which are 10 μm across and are separated by 10 μm.

3.2 Structural Characterization

Scanning electron microscopy (SEM) was used to characterize the surface structure of samples. An in-lens detector was used for more effective tomography characterization, and charges on the surface appear bright. Unexpectedly large agglomerations of molecules on the order of multiple microns were observed, as well as large gaps between adjacent agglomerations. As seen in Fig. 3.2.1(c), the effect of sample degradation from applying too large of an in-plane current caused segregation of the molecules and polymer surface, cracks, and even larger gaps between molecules. This SEM image with large gaps will correspond to the significant change in behavior of the direct current I-V data in Fig. 4.1.1 discussed in the following section.

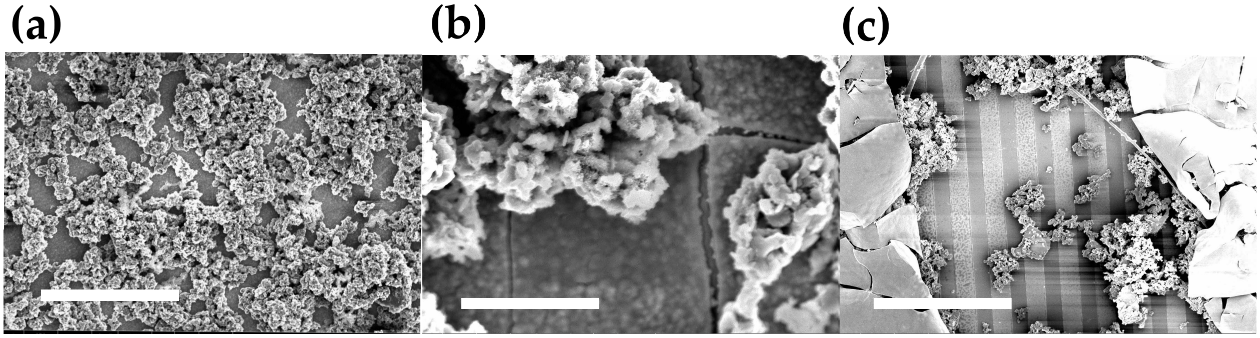

Fig. 3.2.1: *SEM images of non-degraded sample ((a) and (b)) and degraded sample (c). Length scales are 10 μm, 2 μm, and 40 μm, respectively.*

Initial attempts at drop-casting resulted in visibily non-uniform and cracked samples when viewed with SEM. Repeated attempts to mitigate sample degradation through improved drop-casting technique saw improvements in sample quality, but degradation still occurred for small currents in the nA range under an in-plane voltage around 0.5 V. Future work should consider the use of alternative deposition techniques, namely spin-coating to improve the uniformity of samples that may prevent degradation at low currents.

4 Results and Analysis

4.1 Direct Current I-V Measurements

Though the main objective was to characterize frequency-dependent behavior, the direct current (DC) behavior first needed to be determined. The DC current-voltage curves (I-V) curves had unexpected characteristics, with DC conductivity much smaller than expected when compared to the work of collaborators. Additionally, the curves have clear non-ohmic behavior. A significant capacitive behavior is visible in the hysteresis-like shapes of the I-V curves in 4.1.1, which were first swept from a negative to positive and then positive to negative voltage. This hysteresis behavior proves significant to the development of a circuit model for the system.

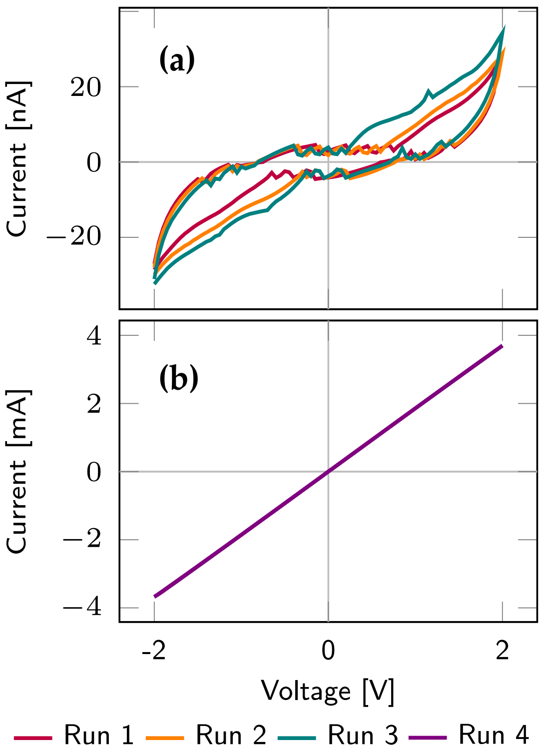

Fig. 4.1.1: *I-V curves for (a) first three runs and (b) a run after the irreversible transition/degradation.*

When taking the I-V curves that resulted in the hysteresis-like patterns, the measurements began at negative voltage. When first crossing 0 V, a negative remanent current remained at 0 V before becoming positive at higher positive voltage values. Similarly, when starting at the maximum positive in-plane voltage applied, a positive remanent current remained at 0 V. This non-Ohmic behavior is demonstrated in Fig. 4.1.1 for measurements taken between -2 V and 2 V. Each curve represents an average over two successive loops. The successive runs 1-4 indicate repeated measurements of such averages. Runs 1-3 show a steady broadening of the I-V loop behavior after successive runs, while run 4 occurs after an irreversible transition to Ohmic behavior with a conductance on the order of magnitude of mS/m compared to the nS/m of previous measurements.

After repeated measurements, the I-V loops increasing widened (runs 1 through 3 in Fig. 4.1.1), with increasing conductivity, before finally transitioning irreversibly from non-ohmic behavior with small currents in the nA range to much larger currents in the mA range following ohmic behavior. This change in conductivity and shape could be due to a crystalline transition in the sample, but the likelihood of sample degradation motivated the restriction of the in-plane voltage range to between ±0.2 V for future samples. For this restricted voltage range, the initial non-ohmic and low conductance behavior is maintained (Fig. 4.1.2). The remanent current motivated investigation of the time evolution of the system while held at different voltage values. Though this restriction is highly limiting, it was necessary to effective characterize the sample in a controlled manner without degradation.

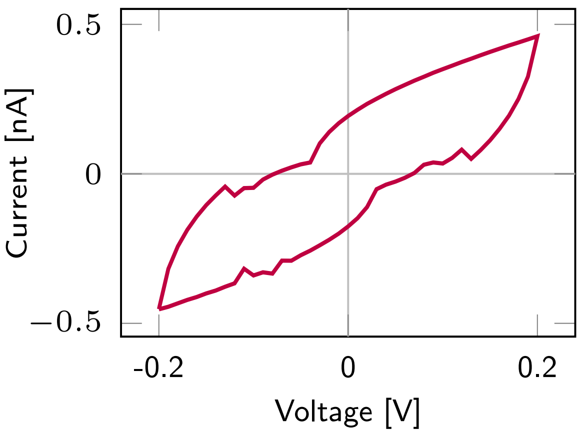

Fig. 4.1.2: *Stable I-V behavior of molecular sample within non-degrading range.*

4.1.1 RC Charging Behavior

Beginning by holding the in-plane voltage at 0.2 V and decreasing in steps of 0.05 V, the time-evolution of the DC current was measured at different voltages. The first three runs (0.2 V, 0.15 V, and 0.1 V) displayed similar asymptotic behavior, but the final run (0.05 V) had a different dip behavior. After analyzing the I-V behavior once again, it was found that the sample had degraded during this run in a manner similar to the transition of the I-V behavior in Fig. 4.1.3

However, when considering the similar asymptotic behavior when held at the first three voltage values, it is apparent that the system displays some sort of charging behavior, though it is not a simple RC charging behavior since the curves are not linear on the logarithmic scale for current.

Regardless, this apparently significant charging behavior justifies the use of an RC circuit model in the analysis of the impedance measurements. Furthermore, it is clear that the specific asymptotic value approached as time progress depends heavily on the voltage value being measured. As such, we assume there is some sort of leakage current in the system. This justifies the the use of a circuit model consisting of a resistor parallel to a capacitor, since such a resistor would have a larger in-plane current across it for a higher voltage once the capacitor becomes fully charged.

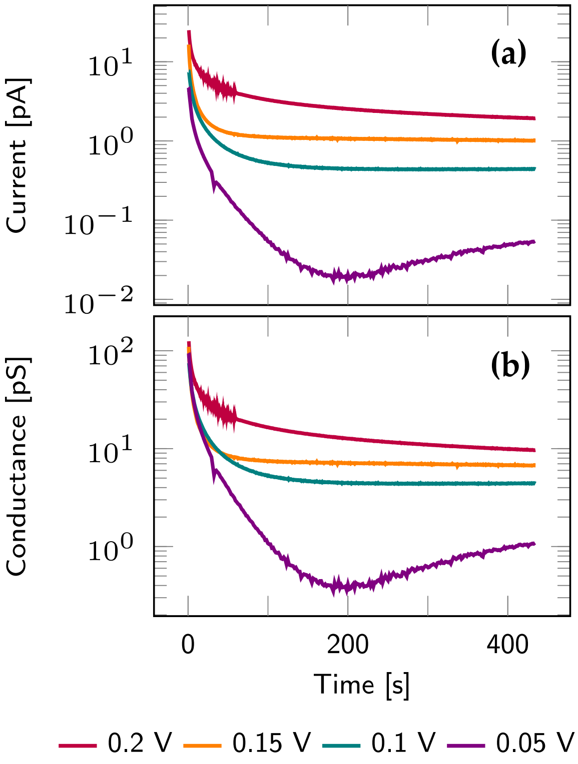

Fig. 4.1.3: *Time-evolution of (a) current and (b) conductance when held at given voltages.*

4.1.2 Circuit Model

With the charging behavior as motivation, we seek to develop a simple RC circuit model that explains, with physical justification, the charging behavior and hysteresis behavior of the I-V curves. The samples have clearly some resistance R, but, based on the charging behavior, they simultaneously function like a capacitor. Since the sample is ideally isotropic, we cannot separate these two circuit elements from one another. We therefore model the sample itself as a resistor of resistance R and capacitor of capacitance C in parallel with one another. Furthermore, we also assume some contact resistance R_c from the electrodes on either side of the sample.

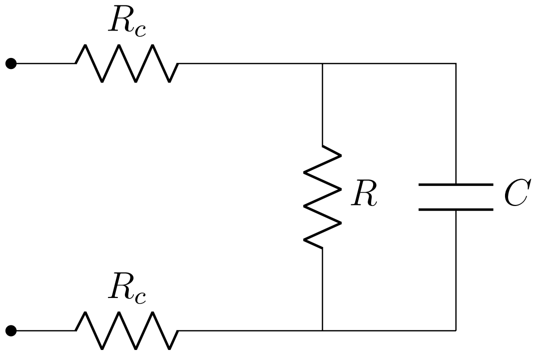

Fig. 4.1.4: *Circuit used to theoretically model the molecular samples.*

From this circuit model, we can easily derive the effective resistance of the system *as measured in the impedance measurements*. From this effective resistance model, we can find the values of R and C for the samples as described in the model.

The two contact resistances, each with resistance R_c, are in series with parallel R and C. For parallel RC impedance Z_{RC}, we have

$$Z = Z_{RC} + 2R_C, \tag{4.1}$$

and

$$\frac{1}{Z_{RC}} = \frac{1}{Z_R} + \frac{1}{Z_C} \tag{4.2}$$

$$= \frac{1}{R} + i\omega C \tag{4.3}$$

$$= \frac{1 + i\omega RC}{R}. \tag{4.4}$$

Substituting for characteristic frequency $\omega_0 = \frac{1}{RC}$, we have

$$Z_{RC} = \frac{R}{1 + i\frac{\omega}{\omega_0}}. \tag{4.5}$$

Then

$$Z = \frac{R}{1 + i\frac{\omega}{\omega_0}} + 2R_C \tag{4.6}$$

$$= \frac{R(1 - i\frac{\omega}{\omega_0})}{(1 + i\frac{\omega}{\omega_0})(1 - i\frac{\omega}{\omega_0})} + 2R_C \tag{4.7}$$

$$= \frac{R(1 - i\frac{\omega}{\omega_0})}{1 + (\frac{\omega}{\omega_0})^2} + 2R_C. \tag{4.8}$$

Noting that $R_{eff} = \mathrm{Re}(Z)$ and $X_{eff} = \mathrm{Im}(Z)$, we have

$$R_{eff} = \frac{R}{1 + (\frac{\omega}{\omega_0})^2} + 2R_C \tag{4.9}$$

and

$$X_{eff} = \frac{-R}{\frac{\omega_0}{\omega} + \frac{\omega}{\omega_0}}. \tag{4.10}$$

We have now found the effective resistance R_{eff} and capacitive reactance X_{eff} as functions of frequency ω. R_{eff} decays algebraically with ω^2 for higher frequencies (relative to ω_0), which corresponds to linear behavior on a logarithmic scale, as it does in the data. Furthermore, X_{eff} implies that the model functions like a *band-stop filter*. For frequencies relatively large or small compared to ω_0, the effective capacitive reactance is predicted to approach zero (not letting such frequencies pass) based on the model. It is noted that only the high frequency limit was tested, and it is currently unknown how the reactance behaves in the low frequency limt. For the large frequency limit, the main range of interest, X_{eff} decays with ω. For very high freqencies, the model approaches the typical capacitive reactance equation for a lone capacitor. To further test the circuit model in the future, it may be interesting to consider low frequencies rather than just higher ones to test the model for effective capacitive reactance since no low frequency impedance data is included here.

4.2 Fitting the Impedance Measurements with Circuit Model

The chosen circuit model is necessary when interpreting the frequency dependent AC behavior, particularly when interpreting the decay of the effective resistance. Measurements were taken for the magnitude and phase of the impedance. Without the derived circuit model, there would be no reason to expect anything other than a constant resistance based on the real part of the impedance. However, the data clearly demonstrates a decay in the real part of impedance, further motivating the use of the model. The model predicts an algebraic decay of a frequency-dependent effective resistance, which is correlates well to the algebraic decay of the real part of the impedance in Fig. 4.2.1, though the rate of decay is lower than predicted. Furthermore, using equation (4.10) for capacitive reactance (the negative of the imaginary part of impedance) returns a consistent value for capacitance at high frequencies when the RC circuit model is used, further indicating its appropriateness. By inspection, it is also clear that this capacitive reactance equation approaches that of a lone capacitor in the high frequency limit.

Fitting to the average value in 4.2.1(c) gives a capacitance value of $C \approx 120$ pF. Using this value in equation (4.9) for effective resistance, we find a value of R of approximately 40 Ω. Then $\omega_0 = \frac{1}{RC} \approx 200$ rad/s.

While unable to demonstrate frequencies beyond 1 MHz, the decay trend at higher frequencies is sufficient when extrapolated from the given data. Extrapolating the impedance behavior to the GHz range, with the impedance magnitude dropping slightly less than an order of magnitude per order of magnitude increase in frequency, we expect a sufficiently small impedance on the order of magnitude of 1 Ω. Thouogh impedance decays quickly, the resistance of 40 Ω from the fit is much higher than previous value of < 1 Ω/cm.

Overall, this results indicate the desired behavior of the AC measurements, with sufficiently fast read/write operations shown by the rapidly decaying impedance in the high frequency limit. There is no noticeable inductive behavior at high frequencies. As such, the Fe(qsal)$_2$-TCNQ$_2$ molecule continue to be a promising candidate for microelectronics.

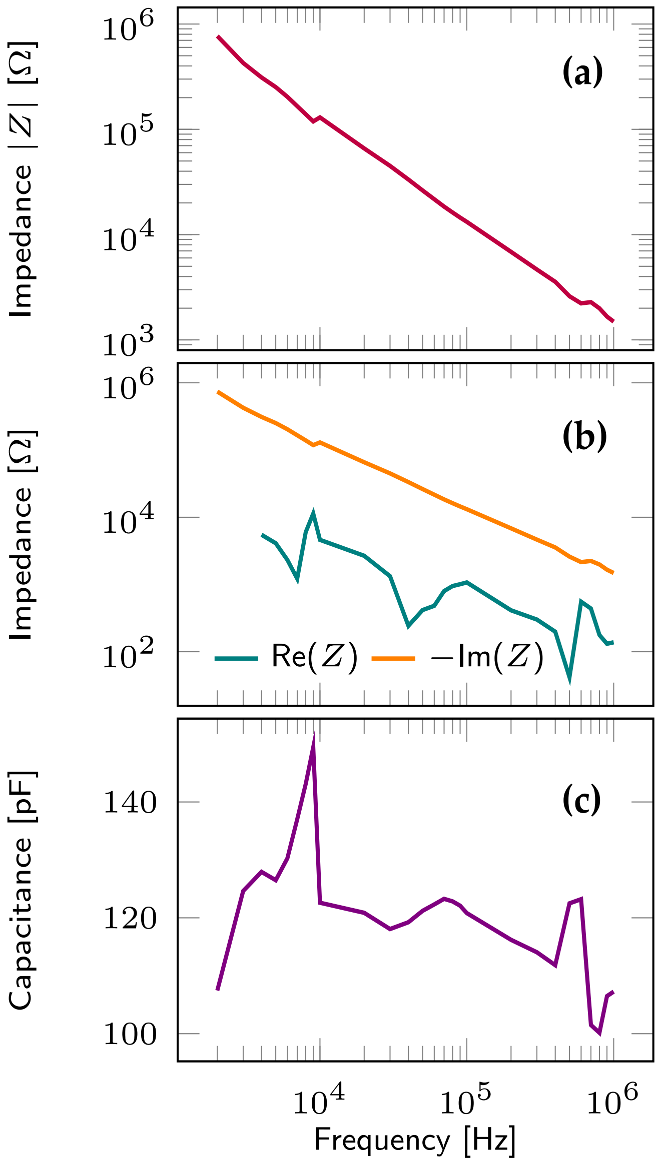

Fig. 4.2.1: *Frequency dependence for (a) impedance, (b) real and imaginary parts (effective resistance and capacitive reactance) of impedance, and (c) capacitance as calculated using equations (4.9) and (4.10) derived from circuit model.*

5 Conclusion and Outlook

Due to the well-performing impedance behavior when extrapolated to the GHz range, the $Fe(qsal)_2(TCNQ)_2$ molecule is still a promising candidate for application in molecular microelectronics. However, a major potential hindrence to further study and application is the apparent tendency for sample degradation when low currents are applied. This work was limited by the necessity to severely limit the in-plane current within the sample. Since the degradation issues seem to be largely connected to sample deposition rather than the specific molecule, it is likely that an improved deposition techniques, such as the use of spin-coating in place of drop-casting, could prevent degradation. To continue work at higher currents, sample quality must be significantly improved to prevent degradation from both higher currents and small, sustanined currents (such as those that caused degradation during the time-evolution measurements).

While the DC behavior yielded unexpected outcomes, many results, such as large leakage current, are marginally impactful at high frequencies. The circuit model can reasonably and effectively be predicted the algebraic decay patterns of both the effective resistance and capacitive reactance equation (4.9) and (4.10). Though this work focuses on high frequency applications in particular, it would be interesting to test this model in the low frequency limit, nearer the characteristic frequency.

Bibliography

[1] T.K. Ekanayaka, R. Streubel, P.A. Dowben et al., Mater. Chem. Phys. 296, 127276 (2023).

[2] P. A. Dowben, D. E. Nikonov, A. Marshall, and C. Binek, Appl. Phys. Lett. 116, 080502 (2020).

[3] K. Ekanayaka, G. Hao, A. Mosey, A. S. Dale, X. Jiang, A. J. Yost, K. R. Sapkota, G. T. Wang, J. Zhang, A. T. N'Diaye, A. Marshall, R. Cheng, A. Naeemi, X. Xu, and P. A. Dowben, Magnetochemistry 7, 37 (2021).

[4] G. E. Moore, "Cramming more components onto integrated circuits," Electronics 38, 114–117 (1965).

[5] Kahn, O.; Martinez, C.J. Spin-Transition Polymers: From Molecular Materials toward Memory Devices. Science 1998, 279, 44–48.

[6] Shvachko, Y.N.; Starichenko, D.V.; Korolyov, A.V.; Kotov, A.I.; Buravov, L.I.; Zverev, V.N.; Simonov, S.V.; Zorina, L.V.; Yagubskii, E.B. The Highly Conducting Spin-Crossover Compound Combining Fe(III) Cation Complex with TCNQ in a Fractional Reduction State. Synthesis, Structure, Electric and Magnetic Properties. Magnetochemistry 2017, 3, 9.

[7] Day, P.; Underhill, A.E. Metal-organic and Organic Molecular Magnets. Phil. Trans. R. Soc. Lond. A 1999, 357, 2849–3184.

Acknowledgements

This thesis was made under the supervision of Professors Robert Streubel and Peter Dowben of the University of Nebraska Department of Physics and Astronomy. Sample deposition and structural characterization were greatly assisted by Wai Kiat Chin at the Department of Physics and Astronomy. Special thanks to Kayleigh A McElveen and the Lai group at the UNL Department of Chemistry for the sythesis and preparation of the molecules.